Parametric study of quarter-wave resonators for sound-proofing building structures

Majid Idrissi[1,*], *Brahim* Lemkalli[2,**], *Abdellah* Mir[3,***], *Abdenbi* Bouzid[1,****], and *Younes* Achaoui[1,†]

[1]Laboratory of Optics, Information Processing, Mechanics, Energetics and Electronics, Department of Physics, Moulay Ismail University, B.P. 11201, Zitoune, Meknes, Morocco
[2]Université de Franche-Comté, Institute FEMTO-ST, CNRS, Besançon, 25000, France
[3]Department of Physics, Moulay Ismail University, B.P. 11201, Zitoune, Meknes, Morocco

Abstract. This study investigates the parametric analysis of a quarter-wave resonator integrated into a brick structure for optimized acoustic isolation in buildings. Starting with a brick of 100 mm thickness and period, the quarter-wave resonator was designed and parametrized. The optimization process yielded significant results, achieving an attenuation of approximately -87 dB with a bandgap width of 82%, surpassing the -72.55 dB attenuation provided by the mass law of the brick alone. These findings highlight the potential of the optimized resonator structure to enhance acoustic isolation, making it a promising solution for noise control in urban environments.

1 Introduction

Acoustic insulation is a crucial issue in urban environments, particularly in residential and commercial buildings, where noise pollution directly affects the comfort of occupants. Traditionally, insulation relies on materials such as hollow bricks and double layers with air spaces, allowing moderate sound attenuation by exploiting the sound-dissipating properties of the trapped air between the walls [1, 2]. However, these conventional techniques reach their limits, especially when managing low frequencies, necessitating innovative approaches to improve efficiency while optimizing space usage [3].

Recently, acoustic metamaterials (AMMs) have garnered significant interest for their unique properties that allow for more efficient and targeted manipulation of sound waves. For example, Lemkalli et al. [4] introduced an innovative design of lightweight panels based on coupled Helmholtz resonators for improving low-frequency acoustic insulation. Their study demonstrated that such panels could achieve broadband noise reduction, particularly in the low-frequency range, by leveraging the resonator geometry to shape the bandgaps. This approach offers a promising solution for improving sound attenuation while maintaining a compact design suitable for modern urban environments, aligning with the growing interest

*e-mail: m.idrisssi@edu.umi.ac.ma
**e-mail: lemkallibrahim@gmail.com
***e-mail: a.mir@umi.ac.ma
****e-mail: ab2.bouzid@gmail.com
†e-mail: achaouiyounes@hotmail.com

in advanced acoustic metamaterials. Baek et al. demonstrated that a Helmholtz resonator-based metamaterial with a fractal structure provides significant sound attenuation over a wide range of frequencies while remaining compact [2]. Similarly, membrane acoustic metamaterials (MAMs) have proven their ability to surpass the mass law, offering high performance in reducing low-frequency noise without adding substantial mass to structures [3]. These AMMs can be applied in complex environments where high levels of sound isolation are needed, such as industrial noise control [3].

In parallel, quarter-wave resonators have emerged as an effective solution for targeting specific frequencies in acoustic insulation. These devices allow for targeted sound absorption at specific resonance frequencies while remaining relatively compact, making them ideal for dense urban environments [5, 6]. Temirova showed that coiled quarter-wave resonators can provide highly efficient low-frequency sound absorption while reducing the required installation space, optimizing their use in confined spaces [7]. Kurecka et al. also employed radially connected quarter-wave resonators in a cylindrical structure to create a pressure drop at specific frequencies, demonstrating the efficiency of this approach both in simulation and experimentation [8].

The practical applications of quarter-wave resonators are diverse. For instance, Qin et al. studied the use of these resonators in thrust chambers, demonstrating that they can effectively control acoustic oscillations by reducing the amplitude of target acoustic modes while dissipating energy through vortices at the resonator's orifice [9]. This approach provides a promising solution for environments where managing acoustic oscillations is crucial. Wang et al. integrated quarter-wave resonators into ventilated windows, achieving a reduction of 10 to 22 dB in a frequency range from 500 Hz to 4 kHz while maintaining natural ventilation, marking a significant advancement for noisy urban settings [10].

Simultaneously, several studies have highlighted the importance of optimizing structures to maximize acoustic performance. Chen et al. proposed a design based on composite membranes to improve sound insulation in industrial applications, while Li et al. explored the use of hybrid metamaterials in construction applications [11, 12]. These studies emphasize the need to combine traditional and innovative solutions to meet acoustic insulation demands across various environments.

Our study aligns with this trend of innovation, proposing an approach to optimize quarter-wave resonators integrated into brick structures to enhance the acoustic insulation of buildings. By using finite element-based numerical modeling techniques, we demonstrate that this approach achieves significant noise attenuation, particularly at low frequencies, while offering a compact solution adaptable to urban environments.

2 Materials and methods

2.1 Design of the Brick and Quarter-Wave Resonator

For this study, we utilized a brick with a period (a) and a thickness (e) of 100 mm. The brick was structured to integrate a quarter-wave resonator designed to enhance its acoustic insulation properties. The resonator's design is based on principles of acoustic metamaterials, aiming to achieve significant sound attenuation within the desired frequency range. The geometry of the setup is illustrated in Figure 1, where the colored section represents the quarter-wave resonator embedded in the brick. The geometric parameters of the resonator, including the width (b) and length (c), are also indicated in the Figure. This structure represents a unit cell, with periodic boundary conditions applied on each side to simulate an infinite array of resonators.

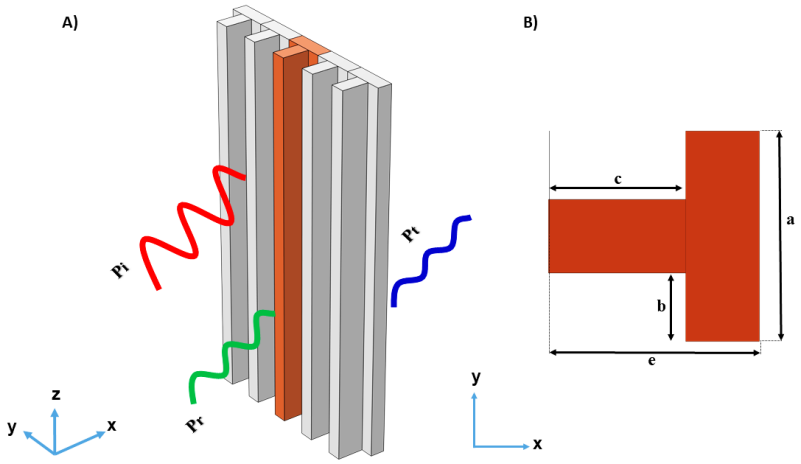

Figure 1. Schematic of the unit-cell cross-section with the integrated quarter-wave resonator within the brick. A) The 3D view illustrates the incident pressure (Pi, red), reflected pressure (Pr, green), and transmitted pressure (Pt, blue), along with the spatial orientation axes (x, y, z). B) The 2D view details the geometric parameters, including the period (a = 100 mm), thickness (e = 100 mm), width (b), and length (c) of the quarter-wave resonator.

2.2 Simulation setup and numerical study

We performed simulations to study the behavior of acoustic waves propagating through the brick structure with the integrated quarter-wave resonator, as shown in Figure 2. These simulations were conducted using finite element analysis software. To mimic experimental conditions, an acoustic plane wave was introduced on one side of the structure. The transmission was assessed by comparing the signal that passed through the brick with the resonator to the incident signal. Due to the periodic nature of the system, the model was limited to a single unit cell, and periodic boundary conditions were applied along the y-axis, as depicted in Figure 2. Perfectly Matched Layers (PMLs) were employed to absorb outgoing waves and prevent reflections at the boundaries, effectively simulating an infinite domain. The physical properties used in the simulation are listed in table 1. The setup involved generating an acoustic plane wave and measuring the sound transmission across the sample using the formula:

$$T\,(\mathrm{dB}) = 20\log\left(\frac{P_t}{P_i}\right) \tag{1}$$

Material	Density (kg.m^{-3})	C_l (m.s^{-1})	C_t (m.s^{-1})
Brick	2000	3073	1882
Air	1.225	343	-

Table 1. Material properties including density, longitudinal wave speed (C_l), and transverse wave speed (C_t).

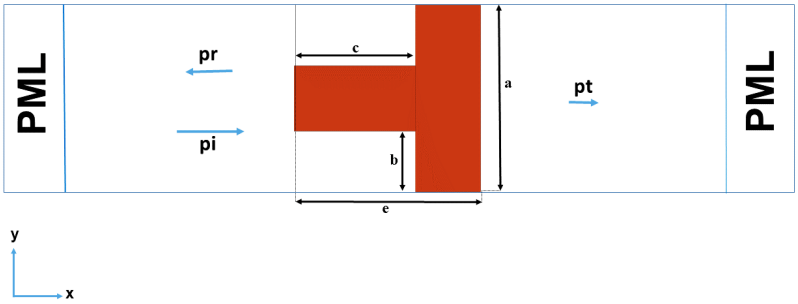

Figure 2. Schematic of the unit-cell cross-section showing the integrated quarter-wave resonator within the brick. The incident pressure (pi), reflected pressure (pr), period (a), and thickness (e) are illustrated

The primary objective of this study is the parameterization of the quarter-wave resonator to optimize its geometry and achieve maximum acoustic attenuation. For each simulation, the width of the resonator (b) was fixed at the minimum and maximum values, 5 mm and 45 mm, respectively. Then, the length of the resonator (c) was systematically varied for each value of b. The transmitted (Pt) and incident (Pi) pressures were extracted from the simulations at different frequencies, and the transmission (T) in dB was calculated using the previously mentioned formula. The transmission results were then normalized to facilitate comparison and analysis. Finally, field maps were plotted to visualize the variation in transmission as a function of frequency, providing a clear and detailed representation of the effect of different parameters on the acoustic performance of the integrated resonator.

This parameterization approach aims to identify the optimal geometric configuration of the quarter-wave resonator, significantly improving the acoustic insulation of building structures. By comparing the results obtained for different values of b and c, we seek to determine the ideal parameters that offer the best sound attenuation. However, while optimizing the resonator dimensions, it is crucial to account for the phenomenon of diffraction, which can significantly impact the overall performance. Diffraction becomes particularly relevant at a frequency where the acoustic wavelength in air matches the periodic structure's dimensions. For the brick under study, with a period of $a = 100\,\text{mm}$, the critical diffraction frequency can be calculated using the relationship between frequency f, wavelength λ, and the speed of sound v in air ($v \approx 343\,\text{m/s}$):

$$f_d = \frac{v}{a} = \frac{343\,\text{m/s}}{0.1\,\text{m}} \approx 3430\,\text{Hz} \tag{2}$$

At this frequency of **3430 Hz**, diffraction effects can disrupt the linear propagation of acoustic waves, leading to a redistribution of acoustic energy and potentially creating "gray zones" or "ineffective zones" where sound attenuation is less effective despite the resonators' design. These zones, characterized by reduced attenuation and compromised acoustic stability, result from the interference patterns induced by diffraction. Considering diffraction is therefore essential for a comprehensive evaluation of the acoustic performance of the resonators. Advanced numerical methods, such as the Finite Element Method (FEM) or the Boundary Element Method (BEM), can be employed to model these complex phenomena. The work by Nico F. Declercq (2013) in On the Fascinating Phenomenon of Diffraction by Periodic Structures[13] serves as a key reference for understanding the mechanisms of diffraction and for developing design strategies aimed at minimizing its negative effects in

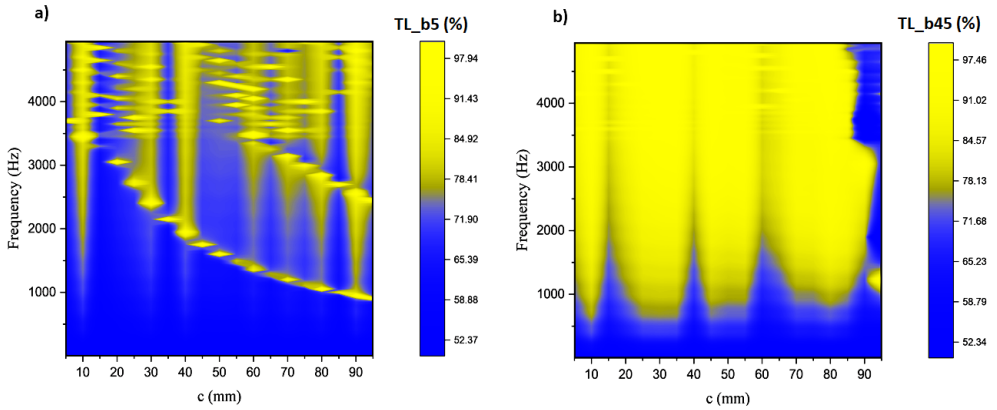

Figure 3. Transmission loss (TL) as a function of resonator length (c) and frequency for different fixed values of resonator width (b). (a) *TL_b5* (%): Transmission loss with *b* fixed at 5 mm. (b) *TL_b45* (%): Transmission loss with *b* fixed at 45 mm. The color scale indicates the transmission loss, ranging from low attenuation (blue) to high attenuation (yellow). The analysis reveals optimal values of *c* for maximum acoustic attenuation, which vary depending on the fixed *b* value.

periodic structures like the one studied here. Incorporating these diffraction considerations before analyzing the simulation results provides a deeper understanding of the potential limitations of the resonators and guides the optimization of their design to maximize acoustic attenuation in frequency bands where diffraction is less influential.

3 Results and discussion

In this study, we employed a systematic, multi-step parameterization approach to optimize the geometry of a quarter-wave resonator integrated into a brick structure to enhance acoustic attenuation. The objective was to determine the resonator's optimal dimensions through comparative analyses of the normalized transmission loss results.

The first step involved fixing the width of the resonator (b) at two specific values—5 mm and 45 mm—representing the minimum and maximum possible configurations, respectively. The length (c) of the resonator was then varied from 5 mm to 95 mm in increments of 5 mm. The results are illustrated in *Figure 3*. For the configuration with $b = 5$ mm (Figure 3a), we observed that certain lengths (c)—specifically 10 mm, 30 mm, 40 mm, 60 mm, 70 mm, 80 mm, and 90 mm—provided significant acoustic attenuation, particularly within the frequency range of 1000 Hz to 4000 Hz. These attenuation peaks indicate that the chosen values of c align well with the natural resonance frequencies of the quarter-wave resonator, leading to effective energy dissipation. In contrast, for $b = 45\,mm$ (Figure 3b), the optimal values for c were found to be between 10 mm and 20–35 mm, as well as between 45–55 mm and 65–90 mm. The broader frequency bands observed in this configuration suggest a more diffuse attenuation effect compared to $b = 5$ mm, which is likely due to increased coupling between the resonator and incident acoustic waves at higher frequencies.

A comparative study of these configurations was conducted by dividing the normalized transmission loss results obtained for $b = 45$ mm by those for $b = 5$ mm (Figure 5e). This analysis demonstrated that the most significant gains in attenuation were found at lengths $c = 35$ mm and $c = 85$ mm, with substantial amplification of attenuation at these values. These

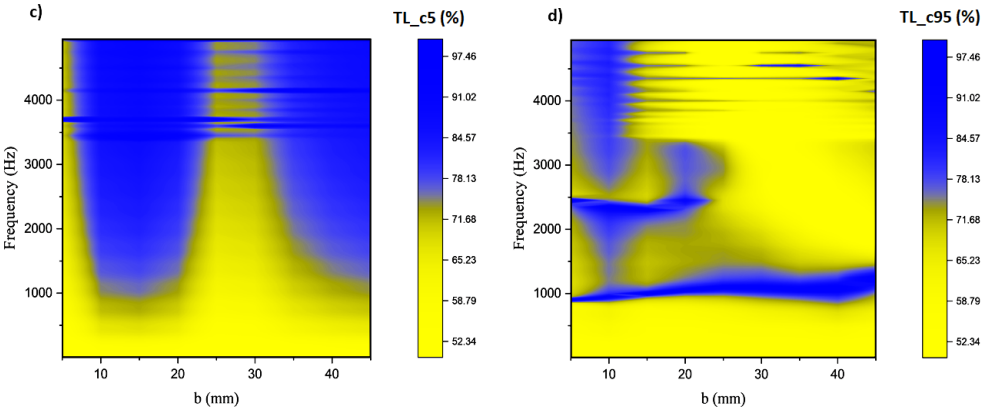

Figure 4. Transmission loss (TL) as a function of resonator width (b) and frequency for different fixed values of resonator length (c). (c) *TL_c5* (%): Transmission loss with *c* fixed at 5 mm. (d) *TL_c95* (%): Transmission loss with *c* fixed at 95 mm. The color scale indicates the transmission loss, ranging from low attenuation (blue) to high attenuation (yellow). The analysis highlights optimal values of *b* for maximum acoustic attenuation, depending on the fixed *c* value.

results highlight that precise tuning of the resonator's length can maximize the performance of acoustic insulation.

In the second step, the length (c) was fixed at its minimum (5 mm) and maximum (95 mm) values, while the width (b) was varied from 5 mm to 45 mm (Figure 4). For $c = 5\,mm$ (Figure 4c), the favorable values of b for achieving maximum attenuation were found to be between 10 mm and 25 mm from 1000 Hz upwards, with another favorable range observed between 35 mm and 45 mm. These results indicate that the resonator's width is crucial in defining the frequency range over which the resonator is most effective, which is consistent with the influence of the resonator's geometry on its natural frequency.

In contrast, for $c = 95\,mm$ (Figure 4d), all widths between 5 mm and 45 mm were found to be favorable for attenuation around 1000 Hz. However, a gap in attenuation was observed between 1000 Hz and 2500 Hz for b values between 5 mm and 25 mm. Figure 5 presents a comparative analysis of acoustic transmission losses for two quarter-wave resonator configurations. In part (5e), the results show the variation in sound transmission as the length c of the resonator is changed, while keeping the width b fixed at 5 mm and 45 mm, respectively. The normalized transmission losses for $b = 45$ mm were divided by those for $b = 5$ mm, revealing key insights into how the resonator's geometry affects sound attenuation. The analysis highlights that for c values between 30 mm and 50 mm, particularly at 35 mm and 85 mm, significant acoustic attenuation is observed. These values correspond to points of enhanced coupling between the resonator and the acoustic wave, resulting in improved insulation performance.

In part (5f), the same comparative approach is applied for varying b, with the length c fixed at 5 mm and 95 mm, respectively. The division of the results for $c = 95$ mm by those for $c = 5$ mm reveals optimal widths for maximizing attenuation, specifically between 20 mm, 25 mm, and 30 mm. This further supports the observation that the combination of width and length is critical in optimizing the resonator's effectiveness in reducing sound transmission. In particular, the analysis suggests that $b = 25$ mm and $c = 85$ mm offer the best coupling and thus the highest sound attenuation, with values reaching up to -87 dB.

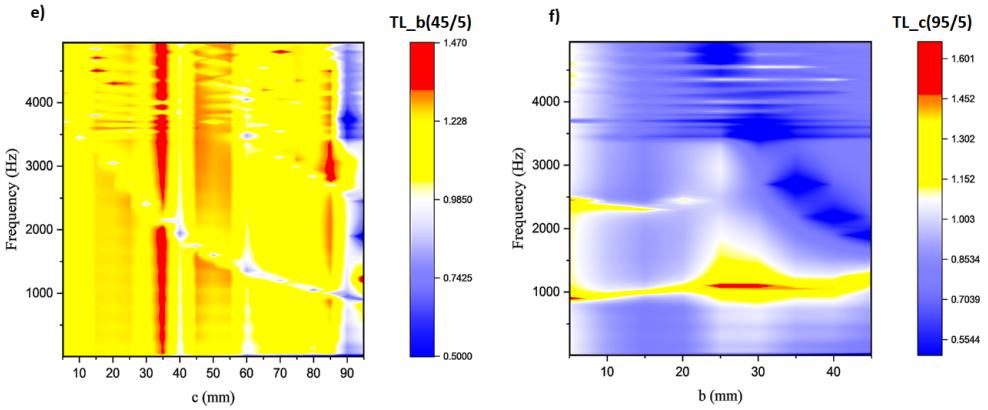

Figure 5. Comparative analysis of transmission loss (TL) for different configurations of resonator width (b) and length (c). (e) *TL_b(45/5)*: Ratio of transmission loss between $b = 45$ mm and $b = 5$ mm as a function of c and frequency. (f) *TL_c(95/5)*: Ratio of transmission loss between $c = 95$ mm and $c = 5$ mm as a function of b and frequency. The color scale indicates the relative change in transmission loss, highlighting regions where specific configurations of b and c lead to enhanced acoustic attenuation.

After determining the optimal values of b and c, transmission curves were plotted for the combinations $c = 35$ mm with $b = 20$ mm, 25 mm, and 30 mm; and $c = 85$ mm with $b = 20$ mm, 25 mm, and 30 mm (Figure 6). The analysis (Figure 6g) shows that the attenuation reaches approximately -120 dB at 2300 Hz for $b = 20$ mm, -130 dB at 2600 Hz for $b = 25$ mm, and -125 dB at 3000 Hz for $b = 30$ mm. These findings indicate that the optimal configuration for achieving the maximum reduction in sound transmission is $c = 85$ mm and $b = 25$ mm, which outperforms mass law predictions, suggesting that the combined effect of the resonator's geometry and the acoustic wave frequency yields superior insulation results.

For $c = 85\,mm$ with $b = 20$ mm and $b = 25$ mm (Figure 6h), we observed the formation of bandgaps centered around 1700 Hz, with attenuations of -78 dB and -87 dB, respectively. These bandgaps are attributed to the *acoustoelastic coupling* between the resonator and the sound wave, which leads to effective trapping and dissipation of sound energy across a range of frequencies.

Observing the transmission curves presented in Figure (7,j), it is evident that increasing the length c of the quarter-wave resonator shifts the acoustic bandgap plateau towards lower frequencies. This phenomenon is further confirmed by the transmission field map illustrated in Figure (7,i). On this map, it is noticeable that the gap initially forms at higher frequencies and gradually shifts to lower frequencies as c increases.

However, diffraction effects were observed around the critical frequency of 3430 Hz due to the periodic structure of the brick (period $a = 100$ mm). This phenomenon, characterized by the redistribution of acoustic energy, created regions where attenuation efficiency was reduced, particularly at higher frequencies. These diffraction-induced "gray zones" represent challenges for the resonator's effectiveness in certain frequency bands. Advanced numerical techniques and further optimization, such as reducing the periodicity of the brick, could potentially mitigate these effects and allow for improved exploitation of high-frequency bandgaps.

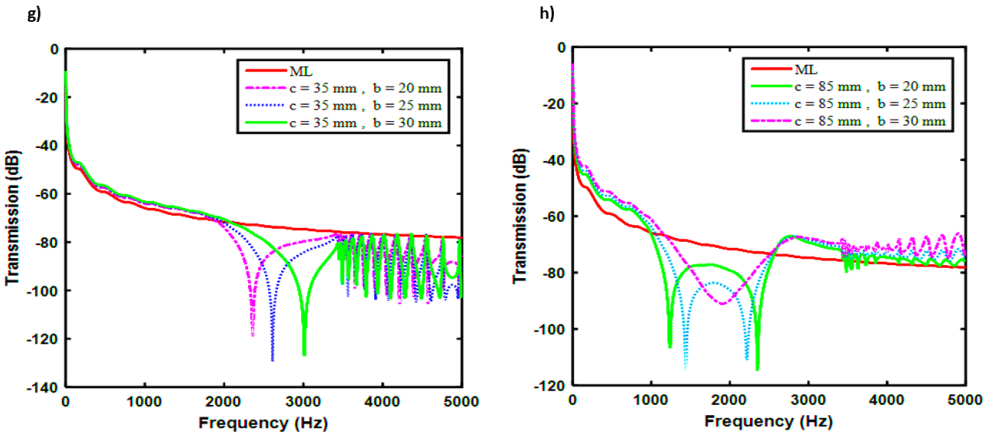

Figure 6. Transmission curves as a function of frequency for different combinations of resonator length (c) and width (b). The left panel shows results for $c = 35$ mm with b values of 20 mm, 25 mm, and 30 mm, while the right panel presents results for $c = 85$ mm with the same b values. The curves compare the transmission loss of each configuration, highlighting the optimal combinations of b and c for maximum acoustic attenuation. The red curve (ML) represents the mass law of the brick without the resonator.

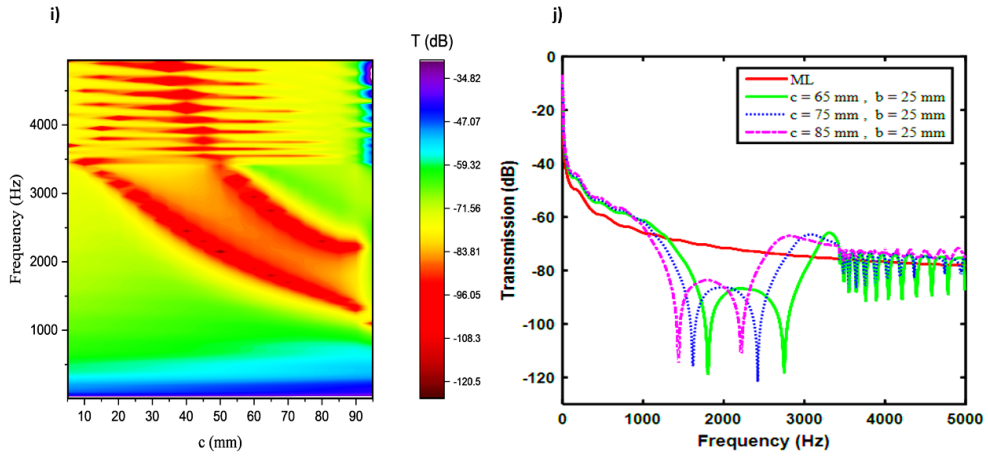

Figure 7. (i) Transmission field map as a function of frequency and resonator length c with a fixed width $b = 25$ mm. The color scale represents the transmission loss (TL) in dB. (j) Transmission curves for different resonator lengths ($c = 65$ mm, 75 mm, 85 mm) with $b = 25$ mm. The curves illustrate how increasing the length c shifts the acoustic bandgap towards lower frequencies, highlighting the impact of resonator dimensions on the transmission characteristics.

4 Conclusion

In this study, we conducted a rigorous parameterization of the dimensions of a quarter-wave resonator integrated into a periodic brick structure to optimize acoustic attenuation. The results demonstrated that the optimal configuration, achieving a maximum attenuation of -87 dB, is obtained with a resonator length of $c = 85$ mm and a width of $b = 25$ mm. This combination effectively creates a significant bandgap, leading to a substantial reduction in sound transmission. However, we observed that further increasing b or c beyond these optimal values results in a decrease in the bandgap's effectiveness, highlighting the importance of precise dimension tuning.

Additionally, the analysis revealed that diffraction, occurring at high frequencies due to the structure's period (100 mm), presents a challenge to broadening the bandgap. To further enhance acoustic performance, reducing the period of the structure could be considered, allowing for better exploitation of high-frequency regions and improved acoustic insulation.

In summary, this study demonstrates that careful tuning of the resonator dimensions and the surrounding structure is crucial for maximizing sound attenuation and enhancing the effectiveness of acoustic materials in noise control applications.

References

[1] R. Lagtayi, L. Lairgi, A. Khouya, A. Daya, E3S Web Conf. **297**, 01933 (2021)
[2] S.H. Baek, J.Y. Jang, K.J. Song, S.H. Park, J. Mech. Sci. Technol. **35**, 2809 (2021)
[3] J. Mo, Z. Peng, X. Wang, Appl. Sci. **12**, 1950 (2022)
[4] B. Lemkalli, M. Idrissi, A. Mir, Y. Achaoui, E3S Web Conf. **469**, 00042 (2023).
[5] J. Chen, J. Qian, Y.J. Guan, Y. Ge, S.Q. Yuan, H.X. Sun, Y. Lai, X.J. Liu, Front. Mater. **8**, 766491 (2021)
[6] X. Li, H. Zhang, H. Tian, Y. Huang, L. Wang, J. Phys. D: Appl. Phys. **55**, 495108 (2022)
[7] K.B. Temirova, Appl. Acoust. **109**, 402 (2023)
[8] J. Kurecka, O. Cepl, V. Han, EPJ Web Conf. **269**, 01030 (2022)
[9] J. Qin, L. Zhou, H. Zhang, B. Wang, Sci. China Technol. Sci. **64**, 397 (2021)
[10] Z.H. Wang, C.K. Hui, C.F. Ng, Appl. Acoust. **75**, 88 (2014)
[11] Y. Medhin, K.A. Khan, Proc. Inst. Mech. Eng. C **236**, 10554 (2022)
[12] K. Miškinis, R. Bliudžius, A. Buska, J. Phys. Conf. Ser. **2654**, 012136 (2023)
[13] Nico Felicien Declercq, *Acoustics Today* **9**, 8–13 (2013).